Journal of Molecular Catalysis A: Chemical 356 (2012) 171–177

Contents lists available at SciVerse ScienceDirect

Journal of Molecular Catalysis A: Chemical

journal homepage: www.elsevier.com/locate/molcata

Highly active Ag/SBA-15 catalyst using post-grafting method for formaldehyde oxidation

Zhenping Qu*, Shijin Shen, Dan Chen, Yi Wang

Key Laboratory of Industrial Ecology and Environmental Engineering (MOE), School of Environmental Science and Technology, Dalian University of Technology, Linggong Road 2, Dalian 116024, China

ARTICLE INFO

Article history:
Received 18 December 2011
Received in revised form 13 January 2012
Accepted 16 January 2012
Available online 25 January 2012

Keywords:
Formaldehyde
Post-grafting
TPD
TPSR
FT-IR

ABSTRACT

The performance of monodispersed Ag/SBA-15 catalyst prepared by post-grafting method was studied. Compared with impregnation method, the catalyst prepared by post-grafting method exhibited higher metal dispersion, smaller silver particle size and better catalytic activity for formaldehyde oxidation. The HCHO can be completely oxidized into CO_2 and H_2O over the silver catalyst at about 100 °C. Temperature programmed surface reaction (HCHO-TPSR) and temperature programmed desorption (HCHO-TPD) experiments demonstrated that the catalyst prepared by post-grafting method exhibited better HCHO adsorption and activated performance at low temperatures. In situ FT-IR spectra revealed that DOM and formate species can be formed on all catalysts, but CO and CO_2 species can only be found on silver supported catalysts and the post-grafting sample trended to form more intermediates. Dynamic test showed that the oxidation of HCHO with gas O_2 can be occurred at lower temperatures on post-grafting catalyst than on other catalysts, which was consistent with the activity test.

1. Introduction

Formaldehyde emitted from buildings, furnishings and decorative materials is becoming a major indoor pollutant in air tight buildings [1]. It is reported that long-term exposure to indoor air even containing a few ppm of formaldehyde may cause nasal tumors, irritation of the mucous membranes of the eyes and skin irritation [2]. Therefore, the abatement of HCHO at moderate temperature is a problem which should be urgently solved.

Catalytic oxidation is a promising technology for the abatement of HCHO because it can be oxidized into CO_2 over catalysts at much lower temperatures than those of thermal oxidation. The conventional catalysts for catalytic oxidation can be classified into three categories: (1) supported precious metals [3,4]; (2) metal oxides and supported non-precious metals [5]; and (3) mixtures of metal oxides and precious metals [6]. Generally speaking, metal oxides and non-precious metals exhibited somewhat low efficiency and shot life span in spite of their availability. Among supported precious metals, silver has been drawing more and more attentions due to its cheapness and high activity for some oxidation reaction at low temperatures [7–11].

Ag/Al_2O_3 catalyst has shown the stable activity for HCHO oxidation above 473 K [12]. Tang et al. reported that Ag supported on MnO_x–CeO_2 exhibited good activity for HCHO oxidation, and the conversion of HCHO was 100% at 373 K [7]. However, most of metal oxides supports are mainly structurally nonuniform, the size and the shape of the obtained metal nanoparticles are hard to be controlled. As we all known, the catalytic performance of the catalysts was directly related to the particle-size and the reaction tends to occur easily on smaller particles [13]. In order to control the particle size, mesoporous silicas was found to be the promising templates to control the shape and size of the occluded metal nanoparticles. Actually, its great high surface area is in favor for a high dispersion of the active component on the surface of the supports as well as increased availability of active sites, which should show a favorable impact on catalytic activity [14]. But few investigations have been devoted to the HCHO oxidation over mesoporous zeolites [15]. In our previous work, it has been found that the MCM-41 mesoporous silica using impregnation method was a relatively good support for HCHO oxidation, and the catalyst with a silver loading of 8 wt.% exhibited high surface reaction activity and good performance as many metal oxides catalysts. However, the particle size of silver was uncontrollable using the impregnation method.

Metal–organic chemical vapor deposition (MOCVD) [16], conventional incipient wetness impregnation and schemes making use of the silanols on the interval channels were the main methodologies for the assembly of metal nanoparticles inside the channels of mesoporous silica [17]. For MOCVD method, the precursors are limited in terms of their high volatility and thermal stability. Impregnation often yields the uncontrolled growth of metal

* Corresponding author.
E-mail addresses: zhenpq@yahoo.com, quzhenping@dlut.edu.cn (Z. Qu).

1381-1169/$ – see front matter © 2012 Elsevier B.V. All rights reserved.
doi:10.1016/j.molcata.2012.01.013

particles both inside the pores and on the external support surface, leading to a board particle size distribution. The use of silanols on the interval channels through silanols functionalization (post-grafting method) to assemble the silver nanoparticles has been proved to be a simple and available method [18]. Compared to the traditional methods, the reducible species and mental ions can be easily anchored on the expected location of supports by the post-grafting method. Furthermore, the obtained catalysts also exhibit small particle size and high dispersity. Zhang and co-workers [19,20] synthesized a novel catalyst using post-grafting method and the catalysts exhibited small particle size (about 5 nm) and high catalytic activity for CO oxidation. Using alkyltrimethylammonium bromide as a modification agent, Mou and co-workers [21] prepared Au/MCM-41 catalysts and the metal particles were mostly embedded within the mesoporous aluminosilicate particles. Moreover, the catalyst still exhibited small particle size even after calcination at 560 °C under air and it show high catalytic activity for CO oxidation.

Generally, SBA-15 mesoporous silica exhibits more stable matrix for forming the occluded nanoparticles due to its thicker wall and larger pore size compared with MCM-41 [22]. Moreover, SBA-type mesoporous materials with the bimodal pore system are expected to be ideal as catalysts and adsorbents. Previous work from other research groups has indicated that SBA-15-type mesoporous silicas have a high affinity for various VOCs due to their complementary micropores [23,24], which will be very important to fabricate dual functional adsorbent/catalyst system for the control of VOCs.

Thus SBA-15 mesoporous silica was used as a host to support silver species in the present work, and a highly dispersed silver nanoparticle catalyst was obtained by post-grafting method. The novel Ag catalyst gave 100% HCHO conversion at 100 °C, as compared to 150 °C with a conventional impregnated Ag/SBA-15 catalyst with a similar silver loading. The formation of intermediates during the HCHO adsorption and oxidation reaction with oxygen on the catalysts and the dynamic changes of the intermediates were also investigated using in situ FT-IR technique.

2. Experimental

2.1. Preparation of supports and catalysts

2.1.1. Materials

The water used in the experiments was deionized with a pure-flow system. 3-Aminopropyltrimethoxysilane (APTS) was used as received from Aldrich in this study. Other organic and inorganic chemicals were supplied by Tianjin Chemical Agent Co. (China). The SBA-15 mesoporous silica used in the experiment was synthesized according to the literature procedure [25].

2.1.2. Preparation of Ag/SBA-15 catalysts

The post-grafting (PG) sample was prepared using silanols functionalization [26]. An amount of 2.0 g SBA-15 was suspended in 120 ml pure toluene and 6.0 ml APTS was added under stirring. The ethoxy groups of APTS could react with hydroxyl groups of SBA-15 and the APTS molecular were anchored on SBA-15 (assigned as APTS-SBA-15). After washed with toluene and then ethanol for several times, the recovered solid was filtered and vacuum-dried at 353 K for more than 6 h. Then the reducing species HCHO was anchored on APTS by stirring 1.0 g APTS-SBA-15 in a 105 ml mixture of formaldehyde, ethanol and deionized water (formaldehyde/ethanol/deionized water = 5:20:80, volume ratio) at 313 K for more than 30 min. The HCHO could react with APTS-SBA-15 to form reducible $NHCH_2OH$ species. The filtered solid was dried at 313 K overnight. To introduce Ag species, the functionalized sample was added into $Ag(NH_3)_2NO_3$ solution and the solution quickly turned to brown or black, which indicated that the silver ions were reduced to silver by $NHCH_2OH$ species. The precipitation was dried at 100 °C for 12 h to get Ag/SBA-15 catalyst. Conventional Ag/SBA-15 catalysts were prepared by the impregnation method (IM) [15]. The silver loading of all the catalysts was about 7 wt.% obtained by ICP (Inductive Coupled Plasma Emission Spectrometer) analysis.

2.2. Catalysts characterization

N_2 adsorption isotherms of the samples were obtained at −196 °C on Quantachrom quadrasorb SI. Before measurement, the samples were treated by degassing at 300 °C for 4 h. The specific surface area was determined by applying the BET method and the average pore size was calculated from the desorption branch of N_2 adsorption isotherms.

X-ray powder diffraction (XRD) patterns were recorded with a Rigaku D/max-γb powder diffractometer using Cu Kα radiation (λ = 0.1542 nm) and operating at 40 kV and 200 mA. The patterns were taken over the 2θ range from 10° to 80° and a position-sensitive detector using a step size of 0.02°.

The TEM pictures were taken on a JEM-2000EX microscope at 100 kV to study the morphology of silver catalysts. Before measurements, the two samples were subject to calcination treatment at 500 °C and suspended in ethanol. Then sample was supported on a copper mesh for the TEM analysis.

2.3. Activity tests

Formaldehyde oxidation was performed in a fixed-bed reactor under atmospheric pressure within a temperature range of 303–423 K. Typically, 0.2 g of catalyst (20–40 mesh) was loaded in a quartz tube reactor. The catalyst was calcined to 500 °C for 2 h in flow of oxygen and cooled down to RT in flow of He prior to the oxidation reactions. Then the HCHO/He stream and O_2/He passed through the reactor, leading to a typical feed gas composition of 1000 ppm HCHO and 15 vol.% oxygen in He. The total flow rate was 50 ml/min, corresponding to a gas hourly space velocity (GHSV) of 15,000 ml/(g_{cat} h). The effluent gases were analyzed on-line by gas chromatograph (Agilent 7890) equipped with TCD and FID detectors. Activity data have been collected at different temperatures in the range of 30–150 °C with a size step increment of 30 °C for each settled temperature which was maintained until steady-state conditions were reached. HCHO conversion was calculated as follows:

$$\text{HCHO conversion}\ \ (\%) = \frac{[\text{HCHO}_{\text{in}}] - [\text{HCHO}_{\text{out}}]}{[\text{HCHO}_{\text{in}}]} \times 100\%$$

where $HCHO_{in}$ and $HCHO_{out}$ stand for the HCHO concentration in the feed gas and effluent gas, respectively.

2.4. Adsorption/desorption and surface reaction experiments

Temperature programmed desorption (HCHO-TPD) and temperature programmed surface reaction (HCHO-TPSR) experiments were performed in fixed-bed reactor system. Typically, 0.1 g of catalyst (20–40 mesh) was loaded in the middle of the reactor and a thermocouple was placed in the middle of the catalyst bed for the temperature measurement. Gaseous HCHO was generated by flowing helium over paraformaldehyde (99.5%, Acros Organics) in an incubator and the HCHO concentration can be changed by varying temperature and flow rate. After calcination at 500 °C for 2 h in flow of oxygen, the catalyst was purged with helium to room temperature (RT), and then gaseous HCHO was passed through the system until it reached saturation. The temperature was ramped at 10 °C/min from RT to 200–300 °C in a flow of helium (TPD) or

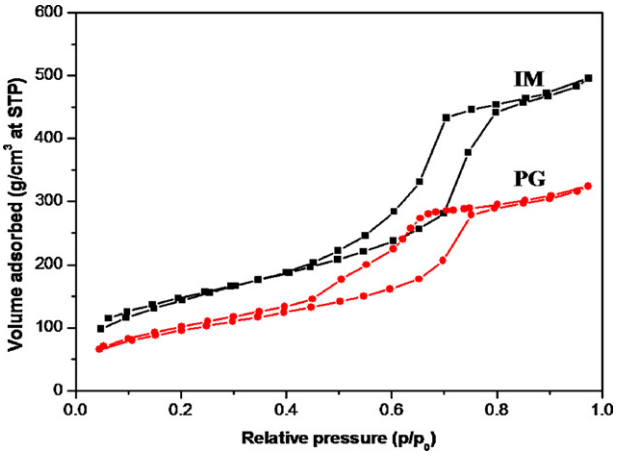

Fig. 1. N_2 adsorption–desorption isotherms for Ag/SBA-15 catalysts.

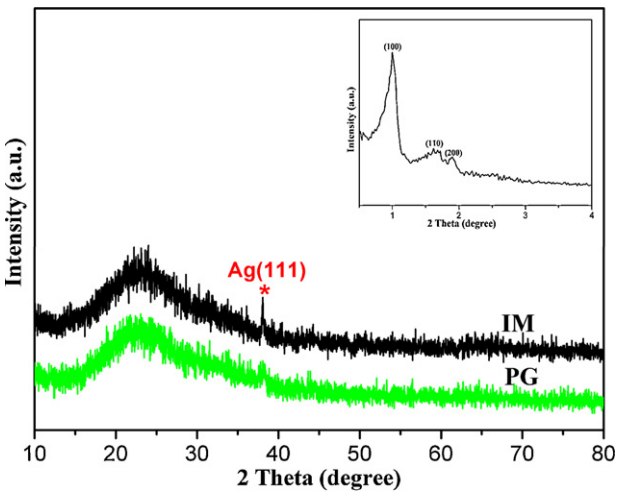

Fig. 2. X-ray diffraction pattern of Ag/SBA-15 catalysts; inset is the small angle XRD patterns of pure support.

oxygen (TPSR) after the catalysts were purged with helium for 1 h to fully remove physically adsorbed HCHO. The effluent gases were analyzed on line by the mass spectrum (Ametek, LC-D200 M).

2.5. In situ FT-IR study

In situ FT-IR transmission spectra were recorded in BRUKER VERTEX 70 equipped with MCT detectors and variable-temperature quartz cells. The catalysts were finely grounded and placed in IR cell-reactor and scanned from 3200 to 1000 cm^{-1} (resolution of 4 cm^{-1}, accumulating 16 scans). A flow of feed gas was controlled by mess flow meters. Before the beginning of the FT-IR experiments, the catalysts were swept by He gas for 1 h at 300 °C. A background spectrum was subtracted from each spectrum, respectively.

3. Results and discussion

3.1. Characterization of catalysts

Fig. 1 shows the nitrogen adsorption isotherms for the Ag/SBA-15 catalysts. Similarly to the nitrogen adsorption isotherms for pure SBA-15 [25], the isotherms of Ag/SBA-15 samples featured hysteresis loops with sharp adsorption and desorption branches. Compared with IM sample, the less sharp desorption branch in the P/P_0 range of 0.4–0.8 indicated a broader mesopore distribution in PG sample. Additionally, the shift of the adsorption branch toward lower pressures in PG sample inferred smaller pore size [27]. Compared with pure SBA-15, the pore size, volume and specific area of silver catalysts was found to be decreased (Table 1) when silver was loaded, PG catalyst especially. Thus it was implied that some silver nanoparticles were induced into the channels of SBA-15 and occupied some pore space [28].

Wide angle XRD patterns of the calcined Ag/SBA-15 catalysts are shown in Fig. 2. For all the samples, the peak appearing at the low angle of $2\theta \approx 22.0^\circ$ corresponds to amorphous silica. The absence of distinct diffraction lines at $2\theta \approx 38.0^\circ$ of silver on PG sample indicated that silver nanoparticles were quite small (under detection limit) or they were in a very high dispersion degree. The small angle XRD pattern of SBA-15 was also displayed (inset of Fig. 2) and we can obviously see three peaks 1 1 0 ($2\theta = 1^\circ$), 1 1 0 ($2\theta = 1.64^\circ$), 2 0 0 ($2\theta = 1.9^\circ$) corresponding to the hexagonal structure of SBA-15. Further investigations about silver nanoparticles and morphology were performed by TEM, as shown in Fig. 3. The direct morphology and size information of silver nanopaticles on the SBA-15 support can be obviously observed. The images are representative for the entire surface of the respective samples and show homogeneous distribution of the silver nanoparticles on the supports.

The TEM images in Fig. 3c and d clearly show the highly ordered parallel cylindrical pore channels of SBA-15, which was in consistent with the SAXD results. We checked the size of at least 150 silver nanoparticles of each sample and the particle size histograms were presented in insets. The average particle size presented in Table 1 was calculated by the method of weighted average from the histogram. Although the post-grafting sample was subject to heat treatment, the silver nanoparticles with an average size of 2.83 nm for PG catalyst were still highly dispersed and confined in the channels of SBA-15 (Fig. 3a and c). The post-grafting method enabled the anchoring of a large number of silver nanoparticles and prevented their aggregation even under a high temperature treatment (500 °C for 2 h) for removing the surfactant. The fact that the channels hindered the aggregation of silver nanoparticles was important in high-temperature reactions, because the sintering of silver nanoparticles can obviously decrease the catalysts activity [29]. Larger metallic silver particles were hardly observed on the PG sample and the results were in accordance with that obtained in XRD patterns. In contrast, for the IM sample, many large particles with size of 10–20 nm deposited on the external surface of the SBA-15 could be observed after high temperature treatment. The remarkable difference between the two samples definitely indicated that the post-grafting method was superior to the impregnation method for obtaining the highly dispersed silver particles.

3.2. Activity test

Fig. 4 shows the conversion of HCHO as a function of temperature over Ag/SBA-15 catalysts. No activity for HCHO oxidation was found on pure support and the active sites for HCHO oxidation were silver sites. The HCHO oxidation activity of Ag/SBA-15 catalysts increased with the reaction temperature, and HCHO can be completely oxidized at 100 °C on the PG sample. However, the 100% HCHO conversion was achieved at 150 °C on the IM catalyst. It is noteworthy that no by-product (such as CO) was detected in the whole activity test. HCHO was completely oxidized to CO_2 and H_2O in oxygen-rich conditions on Ag/SBA-15 catalysts. Thus for the post-grafting method, the high dispersion and narrow size distribution (2–4 nm) of silver nanoparticles may play an important role in improving the catalytic activity. Generally speaking, HCHO oxidation mainly contains four steps according to the Mars-van Krevelen mechanism [30]: adsorption of guest molecules on active sites, activation of guest molecules on active sites, reactions

Table 1
Textural characteristics of the samples.

Sample	Ag[a] (wt.%)	S_{BET} ($m^2\ g^{-1}$)	V_{pore} ($cm^3\ g^{-1}$)	D_{pore} (nm)	Particle[b] size (nm)
IM	7.2	520.6	0.81	6.2	8.08
PG	6.8	347.3	0.54	5.6	2.83
SBA-15	–	746.7	1.37	6.6	–

[a] Attained from ICP.
[b] Attained from TEM image.

between activated HCHO and activated oxygen (O) and desorption of products (H_2O and CO_2). The silver active sites on PG sample may affect some of the three steps and then improve the activity. So the HCHO adsorption/desorption characteristics and its surface reaction activity with oxygen on PG sample were further investigated using temperature programmed technologies.

3.3. Temperature programmed desorption (TPD) and temperature programmed surface reaction (TPSR)

Fig. 5A shows the HCHO desorption curves of Ag/SBA-15 catalysts and pure support. For pure support, there was only one desorption peak (85 °C) which was ascribe to the physically adsorption between HCHO molecules and SBA-15. Due to the stronger adsorption of HCHO on silver species by chemical adsorption [31], the desorption peak obviously moved to higher temperature (90 °C and 96 °C, respectively) when silver was loaded (inset of Fig. 5A). The curve-fitting results showed that the catalysts exhibited two desorption peaks. The desorption peak at lower temperature is ascribed to weak adsorption of HCHO on the support by Van der Waals force, which cannot result in the oxidation reaction. While the desorption peak at higher temperature was attributed to the relatively stronger chemical adsorption between HCHO and silver active sites, which was in favor of the HCHO oxidation. Additionally, it can also be inferred that the adsorption between HCHO and silver active sites is relatively stronger on PG sample than IM sample.

The TPSR results are shown in Fig. 5B. No oxygen consumption is observed for the pure support. But it can be observed for both Ag/SBA-15 samples that the adsorbed HCHO would quickly react with oxygen when the reaction was activated. Both pronounced CO_2 production and consumption of O_2 (inset of Fig. 5B) confirmed the reaction between HCHO and O_2. The PG sample exhibited better surface reaction activity than IM sample and the HCHO can be completely oxidized at 90 °C. For the IM sample, the reaction can

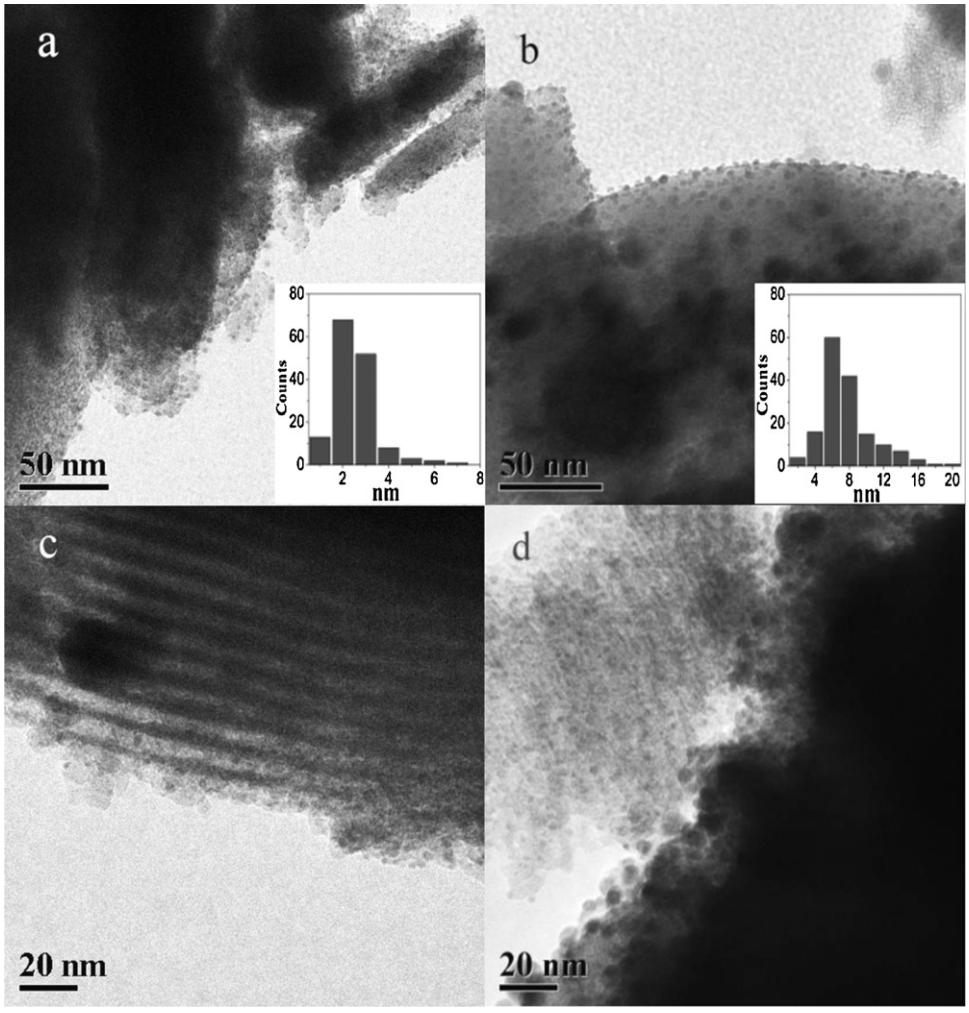

Fig. 3. TEM images of (a, c) post-grafting; (b, d) conventional Ag/SBA-15 catalysts; insets are the particle size histograms according to statistical results.

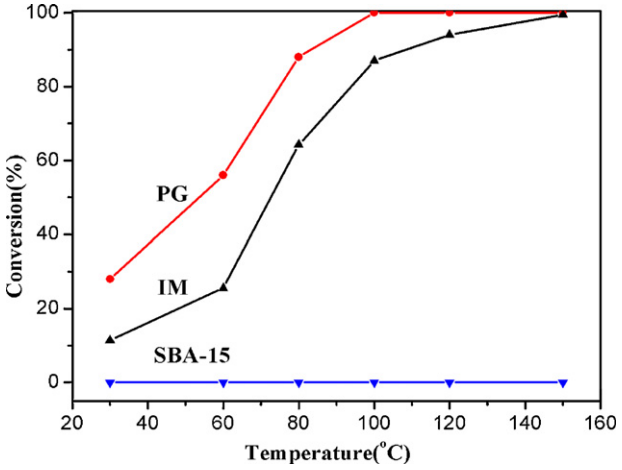

Fig. 4. HCHO conversion on different Ag/SBA-15 samples.

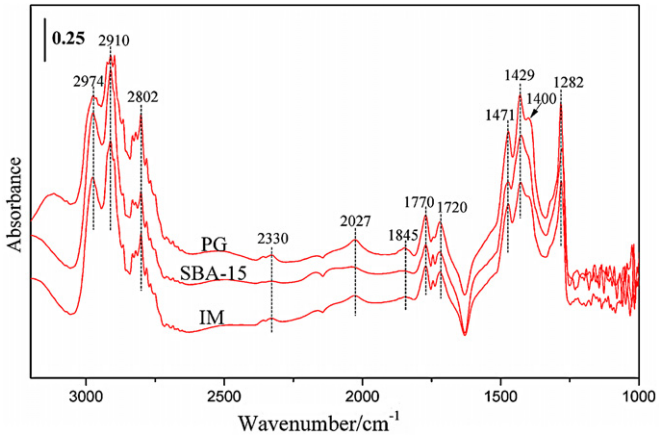

Fig. 6. FT-IR spectra of all catalysts after exposed to a flow of HCHO + He for 60 min.

only be activated at 110 °C. Moreover, the reaction temperature for HCHO oxidation was higher than its desorption temperature for IM sample. As a result, a large amount of HCHO had been desorbed when the IM sample was activated. Thus the amount of CO_2 produced on PG sample was larger than IM sample although more HCHO was adsorbed on the IM sample. The HCHO adsorbed on PG sample showed higher surface reaction activity with oxygen compared with IM sample. In other words, HCHO adsorbed on smaller silver particles is easier to be activated.

3.4. *In situ FT-IR study*

Fig. 6 illustrates the FT-IR spectra of all the catalysts after they are exposed to a flow of He + HCHO for 60 min at room temperature. The bands appearing at 1720–1750 cm^{-1} were ascribed to the HCHO molecules. Apart from HCHO adsorption, the bands observed at 1282 cm^{-1}, 1429 cm^{-1} and 1471 cm^{-1} were assigned to dioxymethylene (DOM). The bands appearing at 2910 cm^{-1} and 1400 cm^{-1} were ascribed to the CH stretching and CH bending of the formate species [14,32]. The obvious adsorption peaks for CO_2 (2330 cm^{-1}) and CO (2027 cm^{-1}) species can be observed on Ag/SBA-15 catalysts. However the adsorption for CO_2 and CO is neglectable for SBA-15 support. The weak adsorption of CO_2 on support might come from the background, because both the activity test and TPSR experiment show that no HCHO oxidation reaction occurred on pure SBA-15 and no CO_2 can be observed by GC and MS. The dioxymethylene, formate and adsorbed CO species were the main reaction intermediates for HCHO oxidation, which was consistent with the previous research [33]. It was revealed that the DOM and formate species can be formed on the catalysts without the help of silver species but the CO_2 and CO species can be formed only on silver catalysts. In this work the formation and dynamic changes of the intermediates were further discussed because the formation of intermediates is usually thought to be essential step for a catalytic reaction [7]. Although the DOM and formate species can be formed on pure support, no activity for HCHO oxidation was observed, as shown in Fig. 4 and the TPSR result. No matter what gases (oxygen or helium) were flowed into the reactor, there is only mutual transformation between intermediates and HCHO and they cannot be further converted into CO_2 even in the presence of oxygen. In other words, HCHO oxidation could not happen on pure SBA-15.

Fig. 7 shows the dynamic changes of the FT-IR spectra of Ag/SBA-15 as a function of temperature (30–150 °C from the top to the bottom curve) in a flow of O_2. In order to give a clear comparison of the dynamic changes, four curves ascribed to 30 °C, 60 °C, 90 °C and 120 °C were marked in red deliberately. The band of intermediates on SBA-15 decreased with temperature increasing (not shown here), but no products were formed. The adsorbed species is desorbed only in the form of HCHO, which was consistent with TPSR results. With the increase of the temperature, the bands intensities of the DOM and formate gradually decreased while the amount of CO is increased at low temperatures (30–60 °C). The TPSR profile

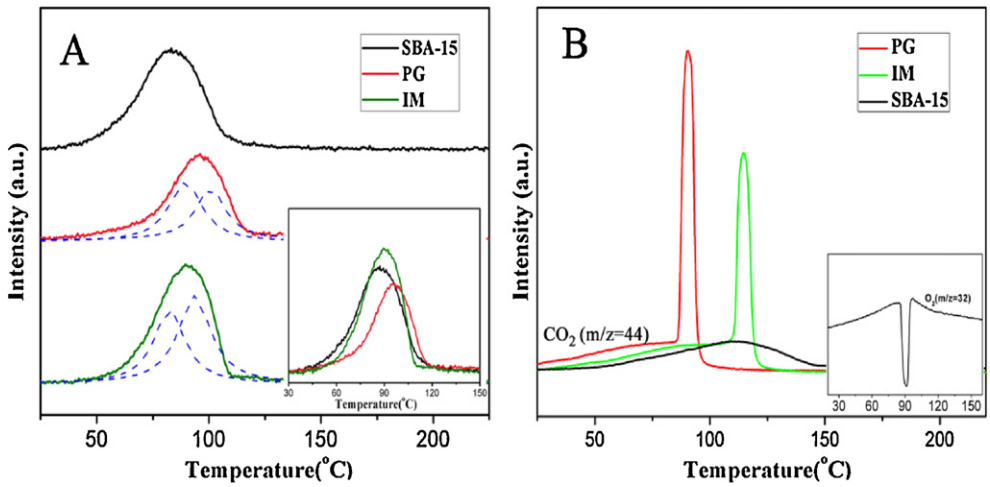

Fig. 5. HCHO-TPD profiles (A) and HCHO-TPSR profiles (B) for Ag/SBA-15 catalysts; insets show the TPD curves and oxygen consumption in TPSR experiment, respectively.

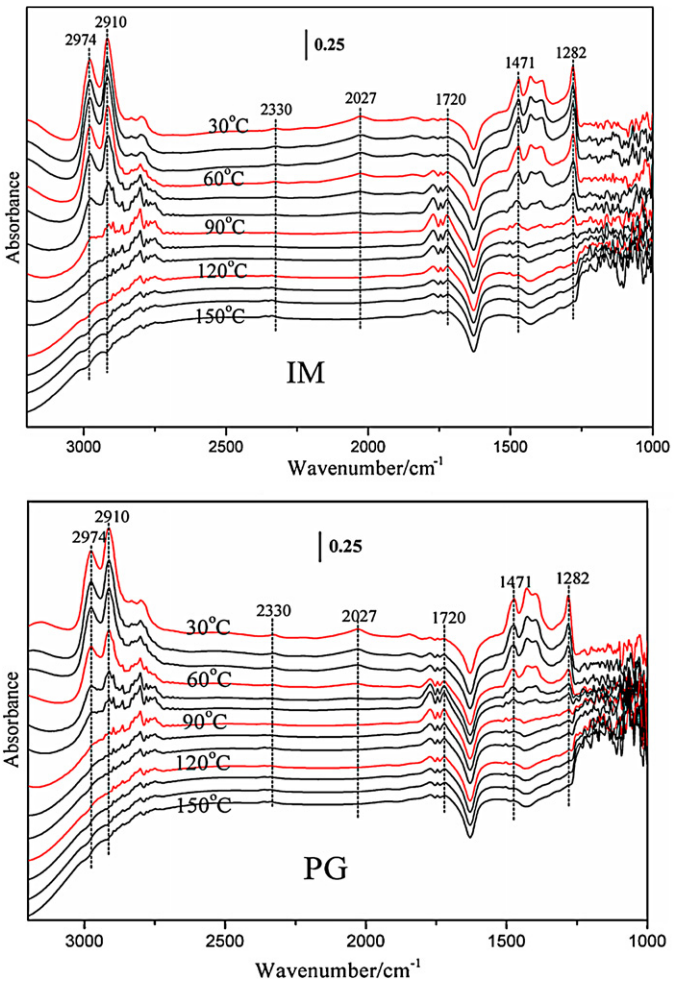

Fig. 7. Dynamic changes of FT-IR of the Ag/SBA-15 catalysts as a function of temperature in a flow of O_2 (30–150 °C from top to the bottom, four curves were marked in red in order to show a clear comparison of the two samples). (For interpretation of the references to color in this figure legend, the reader is referred to the web version of this article.)

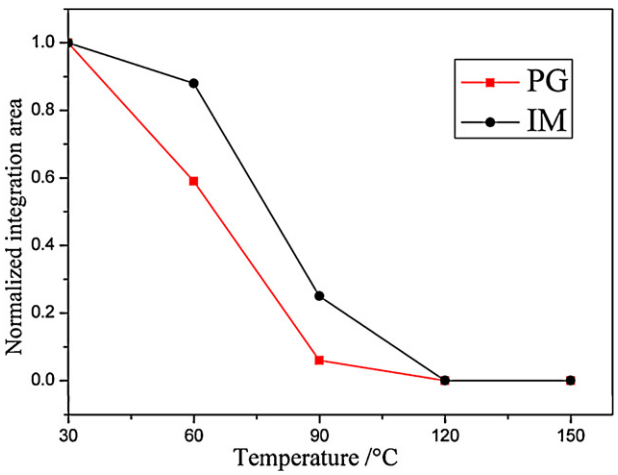

Fig. 8. The relative decrease of intermediates species for the two catalysts as a function of temperature.

also exhibits a sharp desorption peak of CO and the PG sample tend to form more CO at low temperature (not shown in this work). The results revealed that surface formate and DOM species on Ag/SBA-15 can decompose into adsorbed CO species at low temperatures (30–60 °C), which was also found in the previous research [30]. With the further increasing of temperature, CO was rapidly oxidized into CO_2 in the presence of O_2. The weak bands of CO_2 in FT-IR spectra are probably due to the persistent flow of oxygen in the investigation process. It is noteworthy that the bands ascribed to DOM and formate species on PG disappeared faster than IM sample, although the intensity of intermediates on the former is stronger than the latter. In order to show the different performance of the two samples clearly, the integrated peak areas of surface DOM and formate species (1282 cm^{-1}, 2974 cm^{-1} and 2910 cm^{-1}) as a function of temperature was calculated, as shown in Fig. 8. The data shows that the amount of adsorbed DOM and formate species on PG nearly decreased by 40% at 60 °C, but they only decreased by 12% on IM. Moreover, with temperature increasing, the main characteristic peaks for DOM and formate species on PG almost disappeared at about 90 °C, but they still can be observed on IM at the same temperature. Thus it was shown that HCHO adsorbed on PG catalyst was easily oxidized than IM catalyst, which was consistent with the results of the TPSR and activity test.

Catalyst performance is sensitive to the particle size because the surface structure and electronic properties can change greatly in the size range 1–50 nm [34]. As a matter of fact, small silver particles (2–4 nm) exist more active sites, such as steps, kinks, and vacancies [35,36]. According to Wu and Harriott [37], such defects sites on silver crystalline should chemisorb molecules more strongly than other sites. There will be more active sites for smaller particles, and the more intermediates can be formed, which will greatly increase the catalytic activity of catalyst. These results have been ascribed to the available interaction between the reactants and highly dispersed catalysts and it shows the importance of tuning the electronic properties of the metal particles to achieve high catalytic activity.

4. Conclusions

The developed catalyst using post-grafting method exhibits high catalytic activity for HCHO oxidation, with complete HCHO conversion at 100 °C. It was demonstrated for the first time that a 100% HCHO conversion could be attained over a silver catalyst at 100 °C using an inert support (SBA-15). The highly dispersed silver particles with a narrow size distribution and appropriate adsorption intensity between HCHO and active silver sites were contributed to the high catalytic activity of HCHO oxidation. It was found that formaldehyde could convert into DOM and formate ions on the catalysts. No activity for HCHO oxidation was observed on SBA-15 although DOM and formate ions were also was found. The catalytic oxidation cannot take place without the help of silver species. Furthermore, the intensity of the intermediates formed on the novel post-grafting catalyst was stronger than impregnation catalyst, and the intermediates were easier to be activated to form CO_2 with oxygen at lower temperatures. The post-grafting sample was a more efficient catalyst mainly because the catalyst exhibited small particle size and narrow size distribution.

Acknowledgements

This work was supported financially by the National Nature Science Foundation of China (No. 20807010), the Program for New Century Excellent Talents in University (NCET-09-0256), the National High Technology Research and Development Program of China (863 Program) (No. 2009AA062604) and the Specialized Research Fund for the Doctoral Program of Higher Education (No. 200801411111).

References

[1] C. Yu, D. Crump, Build. Environ. 33 (1998) 357–374.
[2] J.J. Collins, R. Ness, R.W. Tyl, N. Krivanek, N.A. Esmen, T.A. Hall, Regul. Toxicol. Pharmacol. 34 (2001) 17–34.
[3] C.B. Zhang, H. He, K. Tanaka, Appl. Catal. B: Environ. 65 (2006) 37–43.
[4] C.B. Zhang, H. He, K. Tanaka, Catal. Commun. 6 (2005) 211–214.
[5] X.F. Tang, Y.G. Li, X.M. Huang, Y.D. Xu, H.Q. Zhu, J.G. Wang, W.J. Shen, Appl. Catal. B: Environ. 62 (2006) 265–273.
[6] C.Y. Li, Y.N. Shen, M.L. Jia, S.S. Sheng, M.F. Adebajo, H.Y. Zhu, Catal. Commun. 9 (2008) 355–361.
[7] X.F. Tang, J.L. Chen, Y.G. Li, Y. Li, Y.D. Xu, W.J. Shen, Chem. Eng. J. 118 (2006) 119–125.
[8] Z.P. Qu, M.J. Cheng, W.X. Huang, X.H. Bao, J. Catal. 229 (2005) 446–458.
[9] X.H. Bao, M. Muhler, B. Pettinger, R. Schlogl, G. Ertl, Catal. Lett. 22 (1993) 215–225.
[10] W.L. Dai, C. Yong, L.P. Ren, X.L. Yang, J.H. Xu, H.X. Li, H.Y. He, K.N. Fan, J. Catal. 228 (2004) 80–91.
[11] Y.B. Yu, X.P. Song, H. He, J. Catal. 271 (2010) 343–350.
[12] C.F. Mao, M.A. Vannice, J. Catal. 154 (1995) 230–244.
[13] T. Schalow, B. Brandt, D.E. Starr, M. Laurin, S.K. Shaikhutdinov, S. Schauermann, J. Libuda, H. Freund, Angew. Chem. Int. Ed. 45 (2006) 3693–3697.
[14] A. Sayari, Chem. Mater. 8 (1996) 1840–1852.
[15] D. Chen, Z.P. Qu, W.W. Zhang, X.Y. Li, Q.D. Zhao, Y. Shi, Colloids Surf. A: Physicochem. Eng. Aspects 379 (2011) 136–142.
[16] K.B. Lee, S.M. Lee, J. Cheon, Adv. Mater. 13 (2001) 517–520.
[17] C.M. Yang, P.H. Liu, Y.F. Ho, C.Y. Chiu, K.J. Chao, Chem. Mater. 15 (2003) 275–280.
[18] L.X. Zhang, J.L. Shi, J. Yu, Z.L. Hua, X.G. Zhao, M.L. Yuan, Adv. Mater. 20 (2002) 1510–1513.
[19] C.H. Tu, A.Q. Wang, M.Y. Zheng, Y. Meng, J.H. Shan, T. Zhang, Chin. J. Catal. 26 (2005) 631.
[20] C.H. Tu, A.Q. Wang, M.Y. Zheng, X.D. Wang, T. Zhang, Appl. Catal. A: Gen. 297 (2006) 40–47.
[21] J.H. Liu, Y.S. Chi, H.P. Lin, C.Y. Mou, B.Z. Wan, Catal. Taday 93–95 (2004) 141–147.
[22] M.T. Bore, H.N. Pham, E.E. Switzer, T.L. Ward, A. Fukuoka, A.K. Datye, J. Phys. Chem. B 109 (2005) 2873–2880.
[23] D.P. Serrano, G. Calleja, J.A. Botas, F.J. Gutierrez, Ind. Eng. Chem. Res. 43 (2004) 7010–7018.
[24] K. Kosuge, S. Kubo, N. Kikukawa, M. Takemori, Langmuir 23 (2007) 3095–3102.
[25] D.Y. Zhao, J. Feng, Q. Huo, N. Melosh, G.H. Fredericson, B.F. Chmelka, G.D. Stucky, Science 279 (1998) 548–552.
[26] J.M. Sun, D. Ma, H. Zhang, X.M. Liu, X.W. Han, X.H. Bao, G. Weinberg, N. Pfänder, D.S. Su, J. Am. Chem. Soc. 128 (2006) 15756–15764.
[27] M. Kruk, M. Jaroniec, Chem. Mater. 12 (2000) 1961–1968.
[28] Y.B. Zhang, Y.N. Shen, X.Z. Zhang, S.S. Sheng, T.N. Wang, M.F. Adebajo, H.Y. Zhu, J. Mol. Catal. A: Chem. 316 (2010) 100–105.
[29] J.X. Peng, S.D. Wang, Appl. Catal. B: Environ. 73 (2007) 282–291.
[30] K.T. Chuang, B. Zhou, S.M. Tong, Ind. Eng. Chem. Res. 33 (1994) 1680–1686.
[31] T. Kecskes, J. Rasko, J. Kiss, Appl. Catal. A 273 (2004) 55.
[32] D. Chen, Z.P. Qu, S.J. Shen, X.Y. Li, Y. Shi, Y. Wang, Q. Fu, J.J. Wu, Catal. Today 175 (2011) 338–345.
[33] C.B. Zhang, H. He, Catal. Taday 126 (2007) 345–350.
[34] A.T. Bell, Science 299 (2003) 1688–1691.
[35] G.A. Somorjai, Introduction to Surface Chemistry and Catalysis, Wiley, New York, 1994.
[36] G. Ertl, Reactions at Solid Surface, Wiley, Berlin, 2009, pp. 21–47.
[37] J.C. Wu, P. Harriott, J. Catal. 39 (1975) 395–402.